Supplementary Materials

for

Using high temporal resolution ambient data to investigate gas-particle partitioning of ammonium over different seasons

Qianyu Zhao[†], Athanasios Nenes[‡,§], Haofei Yu[⊥], Shaojie Song[#], Zhimei Xiao [∇], Kui Chen[∇], Guoliang Shi[†,*], Yinchang Feng[†], Armistead G. Russell[○]

[†] State Environmental Protection Key Laboratory of Urban Ambient Air Particulate Matter Pollution Prevention and Control, Tianjin Key Laboratory of Urban Transport Emission Research, College of Environmental Science and Engineering, Nankai University, Tianjin, 300350, P.R. China.

[‡] School of Architecture, Civil and Environmental Engineering, École Polytechnique Fédérale de Lausanne, Lausanne, CH-1015, Switzerland

[§] Institute of Chemical Engineering Sciences, Foundation for Research and Technology Hellas, Patras, GR-26504, Greece

[⊥] Department of Civil, Environmental and Construction Engineering, University of Central Florida, USA.

[#] School of Engineering and Applied Sciences, Harvard University, Cambridge, Massachusetts 02138, USA.

[∇] Tianjin Eco-Environmental Monitoring Center, P. R. China.

[○] School of Civil and Environmental Engineering, Georgia Institute of Technology, Atlanta, Georgia 30332-0512, USA.

* Corresponding author: Guoliang Shi (nksgl@nankai.edu.cn)

Number of figures: 16

Supplementary Text I. PMF/ME2 calculation method.

Supplementary Text II. Boltzmann fitting patterns in sensitivity regime maps.

Figure S1. Theoretical "Reversed-S" (a) and "S" (b) curve relationships between (a) $\varepsilon(NH_4^+)$ and pH; (b) $\varepsilon(NO_3^-)$ and pH.

Figure S2. The factor profiles modeled by PMF on ME2. ($\mu g/m^3$)

Figure S3. Source contributions' (%) impacts on NH_4^+-NH_3(g) in summer. (a) SN; (b) SS; (c) Coal; (d) Vehicle; (e) Dust.

Figure S4. The impact of meteorological conditions, ion concentrations ($\mu g/m^3$), and pH and $\varepsilon(NO_3^-)^*$ on NH_4^+-NH_3(g) in summer. (a) T(K); (b) RH(100%); (c) $[NO_3^-](\mu g/m^3)$; (d) $[SO_4^{2-}](\mu g/m^3)$; (e) $\varepsilon(NO_3^-)^*$.

Figure S5. $\varepsilon(NH_4^+)$ as a function of pH, with color scales corresponding to source contributions (%) in summer. (a) SN; (b) SS; (c) Coal; (d) Vehicle; (e) Dust.

Figure S6. $\varepsilon(NH_4^+)$ as a function of pH, with color scales corresponding to temperature (K) in summer.

Figure S7. $\varepsilon(NH_4^+)$ as a function of pH, with color scales corresponding to relative humidity in summer.

Figure S8. $\varepsilon(NH_4^+)$ as a function of pH, with color scales corresponding to water content ($\mu g/m^3$) in summer: (a) $\varepsilon(NH_4^+)$ as observed, (b) $\varepsilon(NH_4^+)^*$ as modeled by ISORROPIA-derived values ($[NH_4^+]$ concentrations were calculated by ISORROPIA-II).

Figure S9. $\varepsilon(NH_4^+)$ as a function of pH, with color scales corresponding to (a) $\log(\gamma(H^+))$, (b) $\log(\gamma(NH_4^+))$, (c) $\log(\gamma(NO_3^-))$, (d) $\log(\gamma(SO_4^{2-}))$ in summer.

Figure S10. $\varepsilon(NH_4^+)$ as a function of pH, with color scales corresponding to RH (%) and Boltzmann fitting line of (a) summer sample $\varepsilon(NO_3^-)^*$ constrained from 0.7 to 0.8, (b) all three season (spring, summer, winter) samples within a certain range of $\varepsilon(NO_3^-)^*$ (0.8-0.95) and RH (>36%).

Figure S11. Sensitivity regime map for pH, HNO_3 and NH_3: (a) all year (summer, winter, spring), (b) summer, (c) winter, (d) spring.

Figure S12. Sensitivity regime map of aerosol pH to NH_3 and HNO_3 for samples from the entire sampling period. The dotted lines show the sensitivity of temperature on the sensitivity regime map. The solid lines are calculated by average temperature of all samples, while the dotted lines are calculated by average temperature minus or plus the standard deviation of temperature of all samples.

Figure S13. Joint source-NH_3/HNO_3 sensitivity of aerosol pH to NH_3 and HNO_3 for samples from summer. **(a)** Coal, **(b)** Dust, **(c)** Vehicle, **(d)** SN **(e)** SS.

Figure S14. Joint source-NH_3/HNO_3 sensitivity of aerosol pH to NH_3 and HNO_3 for samples from spring. **(a)** Coal, **(b)** Dust, **(c)** Vehicle, **(d)** SN **(e)** SS.

Figure S15. Joint source-NH_3/HNO_3 sensitivity of aerosol pH to NH_3 and HNO_3 for samples from winter. **(a)** Coal, **(b)** Dust, **(c)** Vehicle, **(d)** SN **(e)** SS.

Figure S16. Sensitivity regime map of aerosol pH to NH_3 and HNO_3 for samples from the entire sampling period. The black points are data collected from all year. The yellow points represent the data applied in Boltzmann fitting ($\varepsilon(NO_3^-)$* (0.8-0.95) and RH (>36%))

Supplementary Text I

PMF/ME2 calculation method.

The PMF/ME2 model calculates an enhanced object function $\boldsymbol{Q_{enh}}$ (Eq 2), where the additional term $\boldsymbol{Q_{\partial ux}}$ was the prior information that was incorporated into the model in the forms of auxiliary equations[9, 66, 67]. The equation is written as follows:

$$Q_{enh} = Q_{main} + Q_{\partial ux} \qquad (Eq.1)$$

$$Q_{main} = \sum_{i=1}^{n}\sum_{k=1}^{m}({}^{e_{ik}}/_{\sigma_{ik}})^2 \qquad (Eq.2)$$

$$x_{ik} = \sum_{j=1}^{p} g_{ij}f_{jk} + e_{ik} \qquad (Eq.3)$$

One of the common auxiliary equations is a "pulling equation" that "pulls" f_{pk} (for instance) toward the specific target value ∂_{pk}:

$$Q_{\partial ux} = \frac{(f_{pk} - \partial_{pk})^2}{\sigma_{pk}^{\partial ux^2}} \qquad (Eq.4)$$

where $\sigma_{pk}^{\partial ux^2}$ is the uncertainty associated with the pulling equation. This term is set by users and reflects the confidence of users in the equation; f_{pk} is the element of factor loading. The information of the performance PMF/ME2 can be found in our previous work[9].

Supplementary Text II

We filtered the points in Boltzmann fitting plot (points in Figure 3(b)), and then highlighted them in the joint source-NH_3/HNO_3 sensitivity regime map (Figure S14). We found that the points (yellow points) tend to follow an almost parallel trend to the blue line (the boundary of HNO_3 sensitive region). The blue line is calculated theoretically by assuming $\varepsilon(NO_3^-) = 0.1$. The yellow points is the sampled flited by $\varepsilon(NO_3^-)^*$ (0.7-0.8). Thus, the yellow points showed parallel trend to the blue line.

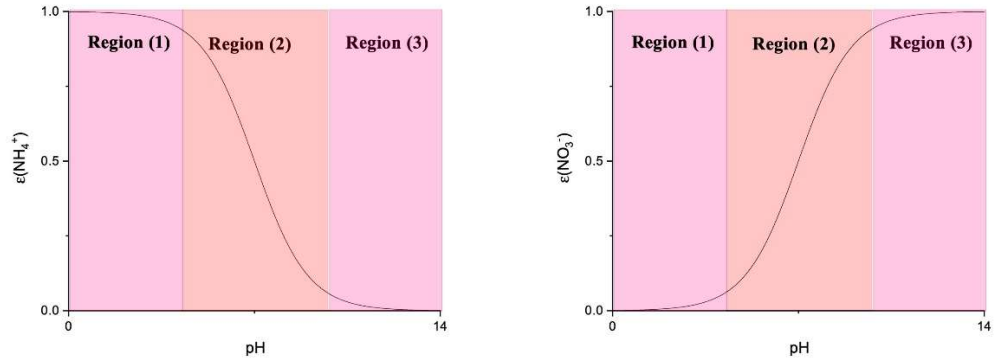

(a) (b)

Figure S1. Theoretical "Reversed-S" (a) and "S" (b) curve relationships between (a) ε(NH_4^+) and pH; (b) ε(NO_3^-) and pH. (The curves are conceptual)

ε(NH_4^+)=NH_4^+ /(NH_4^++NH_3(g))

ε(NO_3^-)=NO_3^- /(NO_3^-+HNO_3(g))"

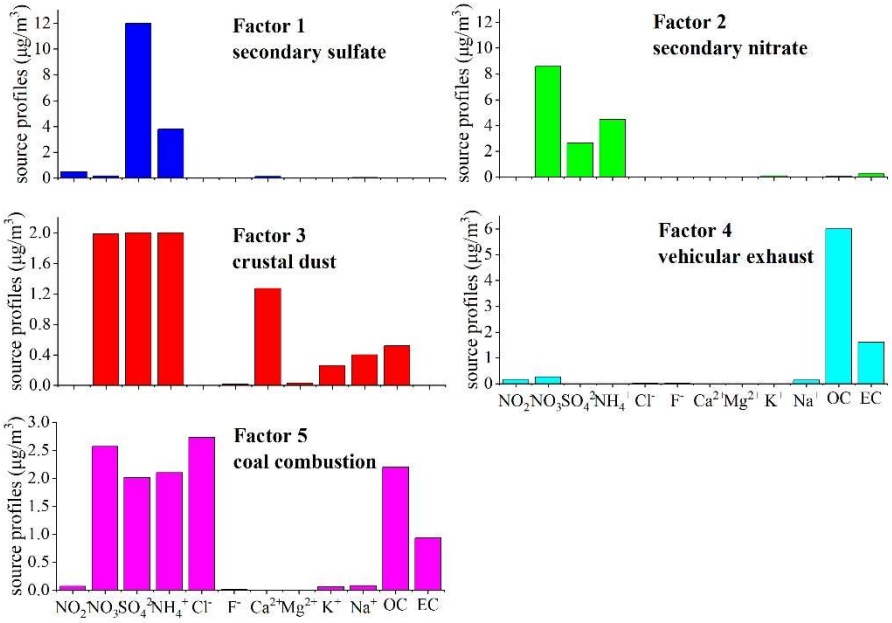

Figure S2. The factor profiles modeled by PMF on ME2. (μg/m^3)

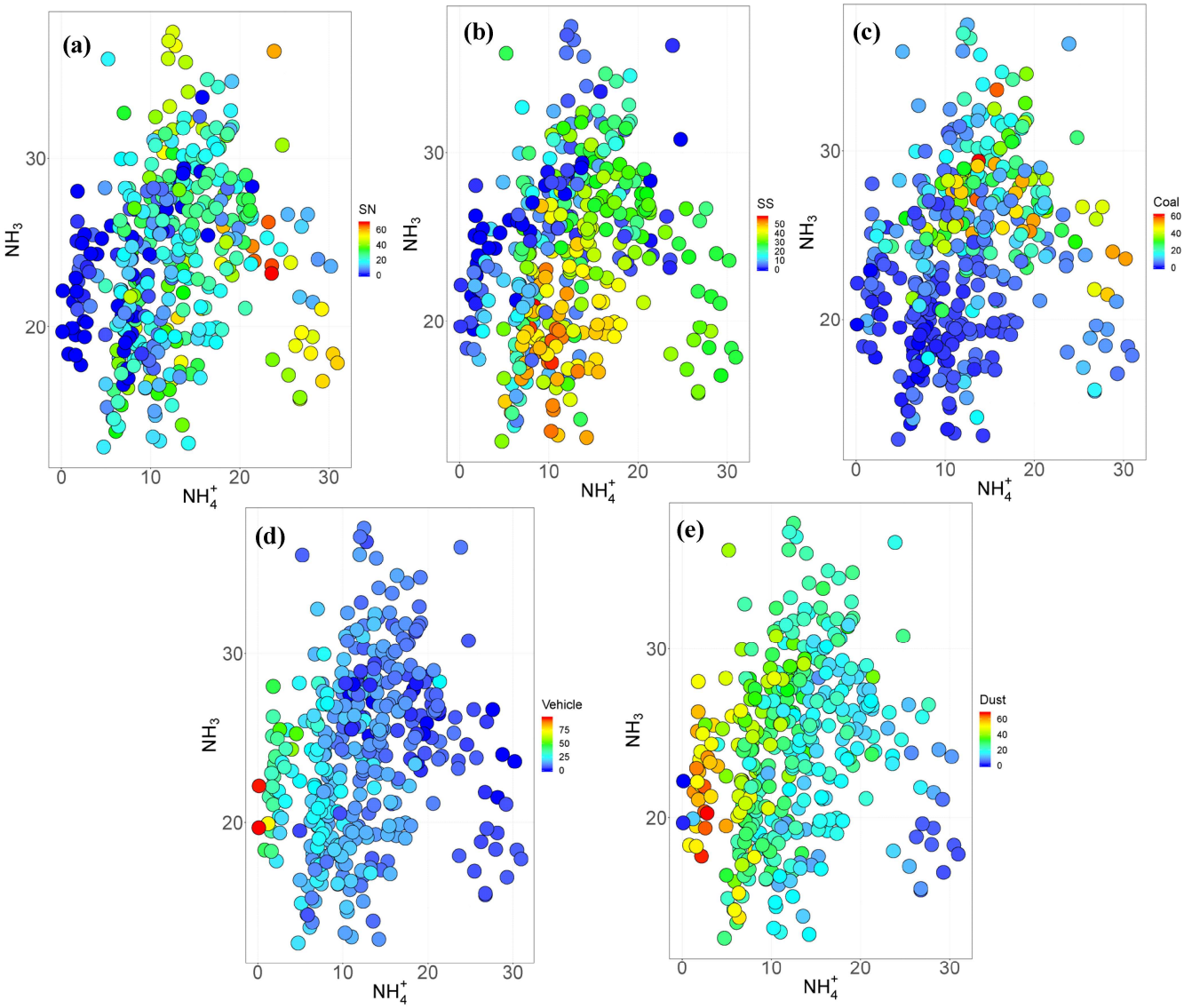

Figure S3. Source contributions' (%) impacts on NH_4^+-NH_3(g) in summer. (a) SN; (b) SS; (c) Coal; (d) Vehicle; (e) Dust.

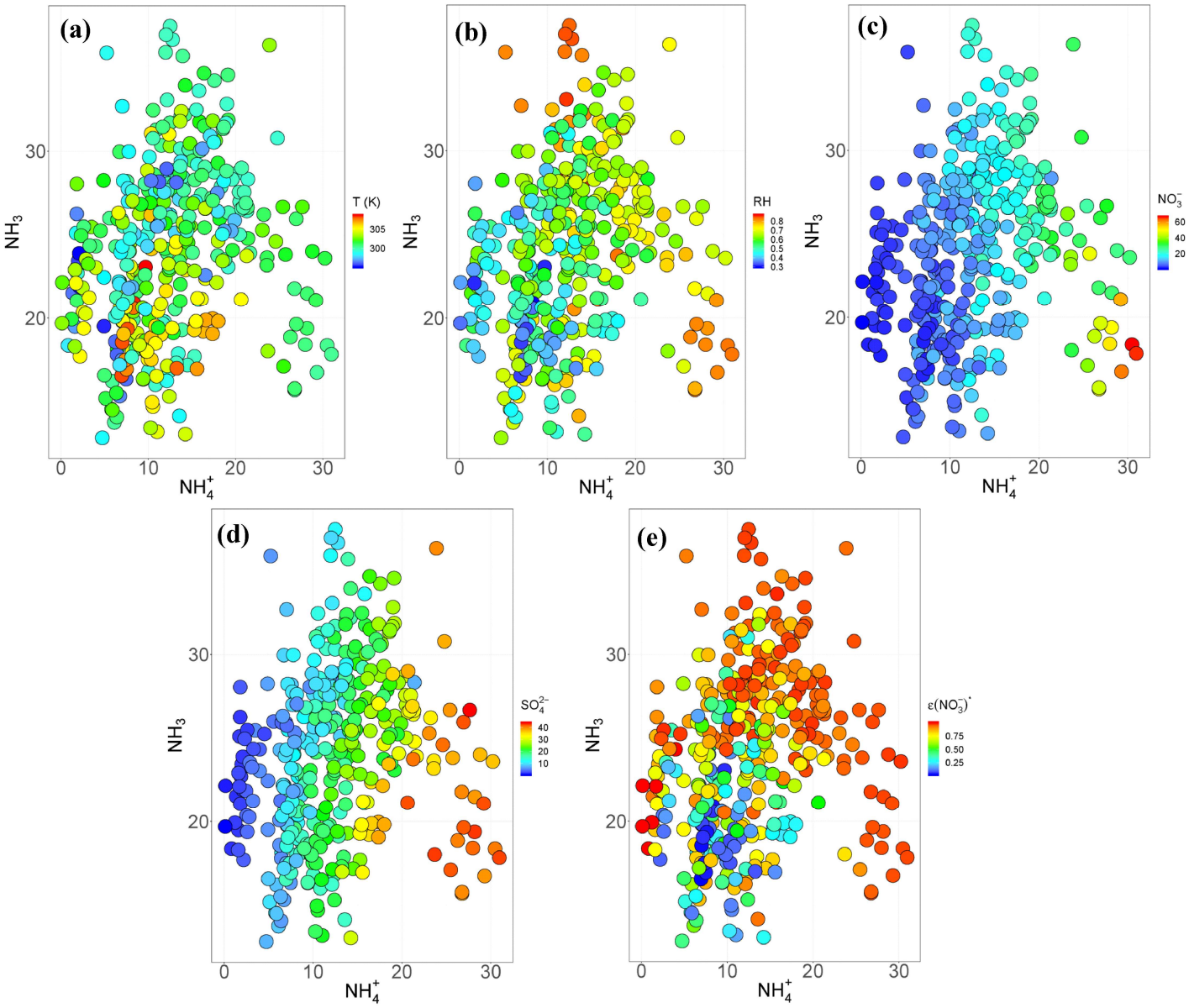

Figure S4. The impact of meteorological conditions, ion concentrations (μg/m^3), and ε(NO_3^-)* on NH_4^+-NH_3(g) in summer. (a) T(K); (b) RH(100%); (c) [NO_3^-](μg/m^3); (d) [SO_4^{2-}](μg/m^3); (e) ε(NO_3^-)*.

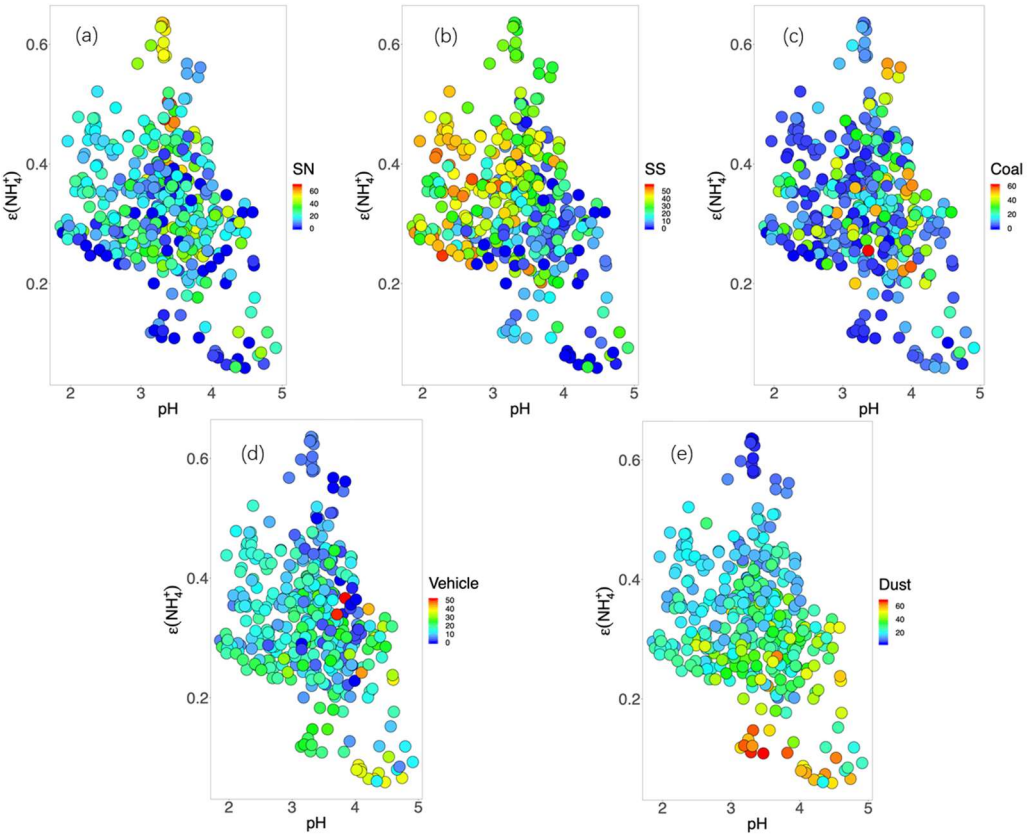

Figure S5. ε(NH_4^+) as a function of pH, with color scales corresponding to source contributions (%) in summer. (a) SN; (b) SS; (c) Coal; (d) Vehicle; (e) Dust.

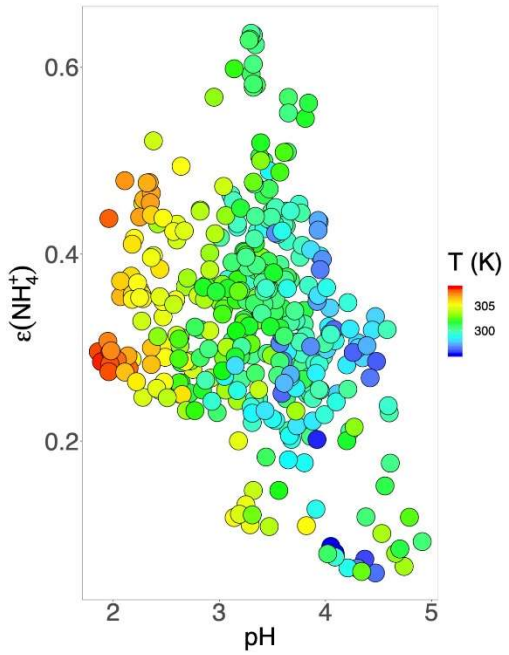

Figure S6. ε(NH_4^+) as a function of pH, with color scales corresponding to temperature (K) in summer.

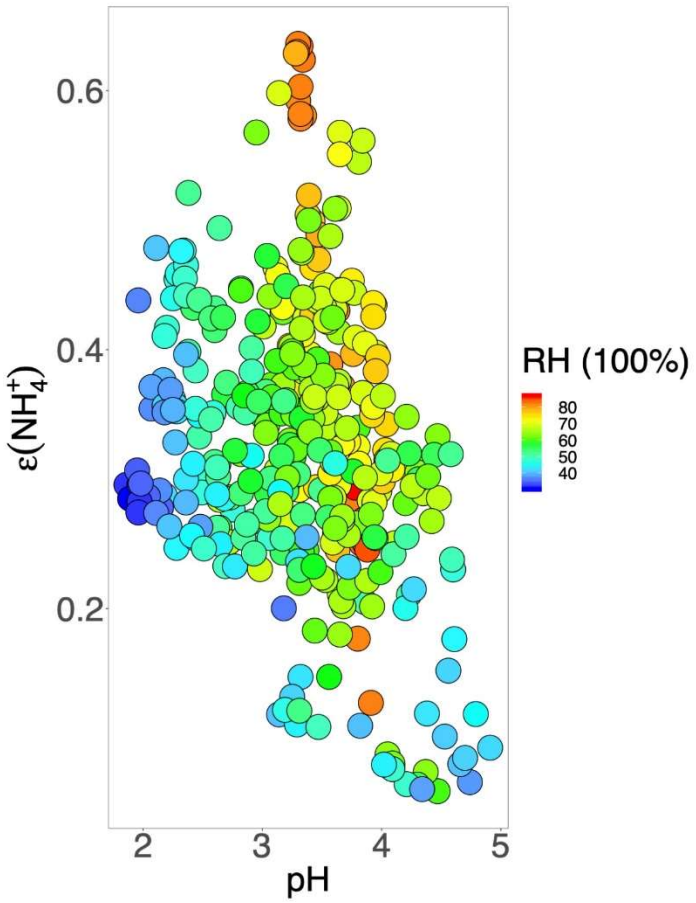

Figure S7. ε(NH_4^+) as a function of pH, with color scales corresponding to relative humidity in summer.

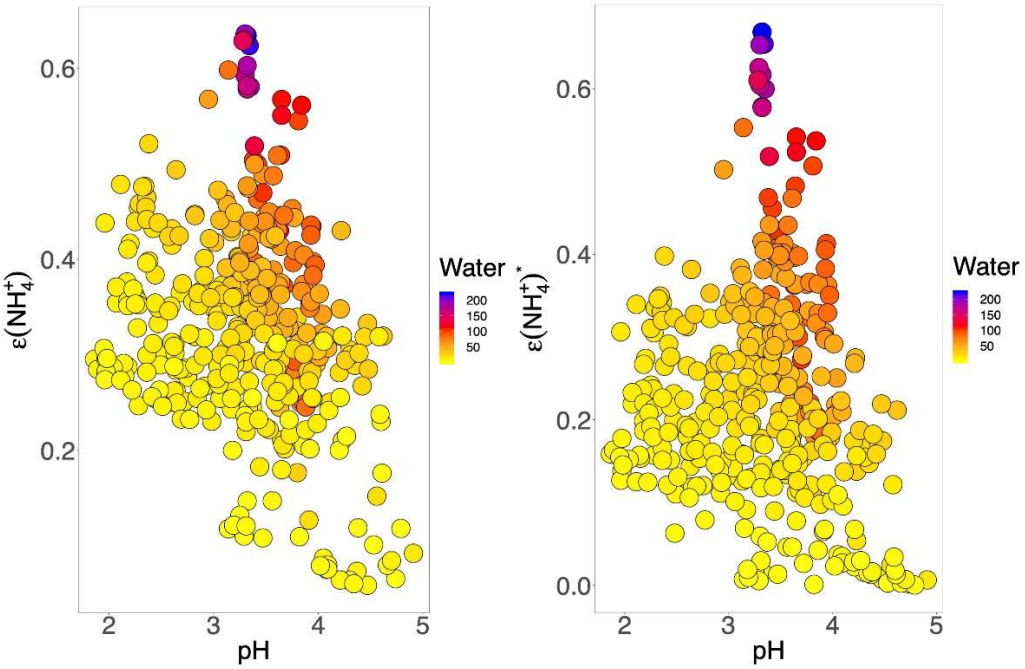

Figure S8. $\varepsilon(NH_4^+)$ as a function of pH, with color scales corresponding to water content ($\mu g/m^3$) in summer: (a) $\varepsilon(NH_4^+)$ as observed, (b) $\varepsilon(NH_4^+)^*$ as modeled by ISORROPIA-derived values ($[NH_4^+]$ concentrations were calculated by ISORROPIA-II).

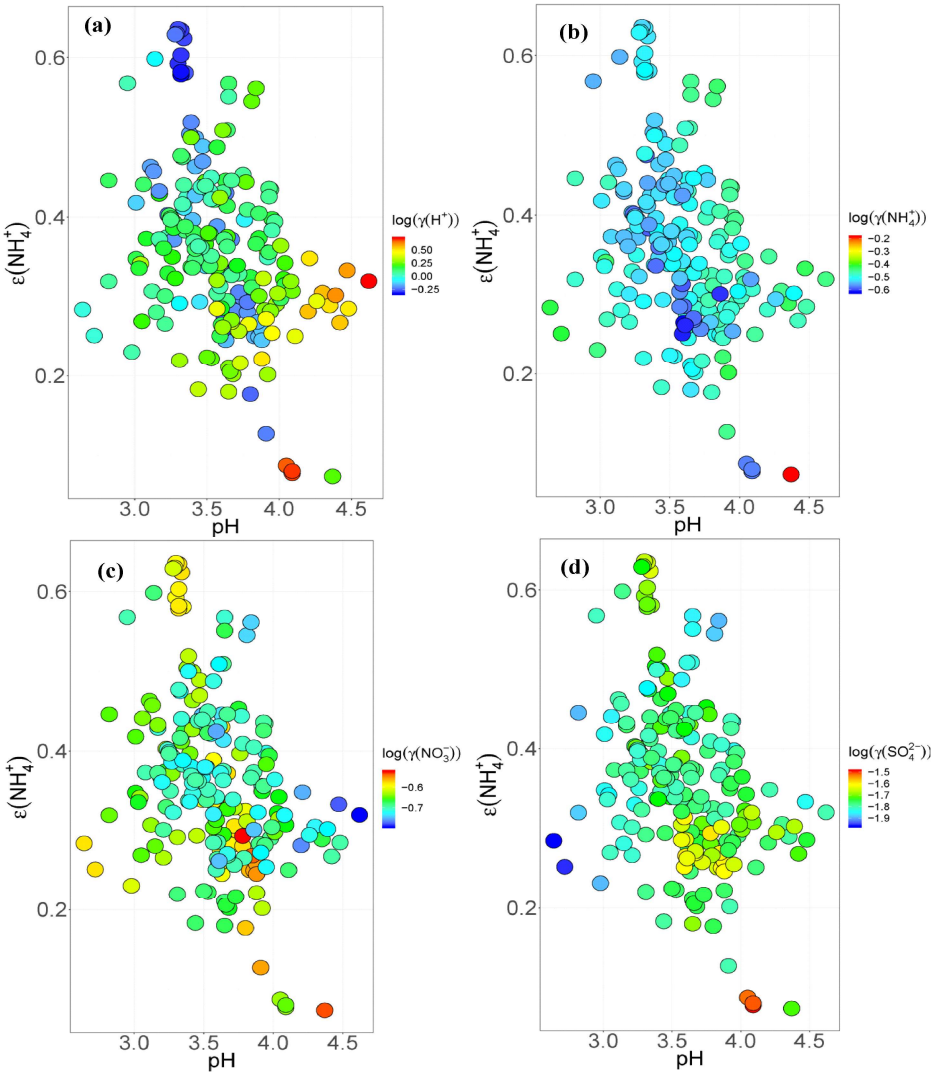

Figure S9. ε(NH_4^+) as a function of pH, with color scales corresponding to (a) log(γ(H^+)), (b) log(γ(NH_4^+)), (c) log(γ(NO_3^-)), (d) log(γ(SO_4^{2-})) in summer.

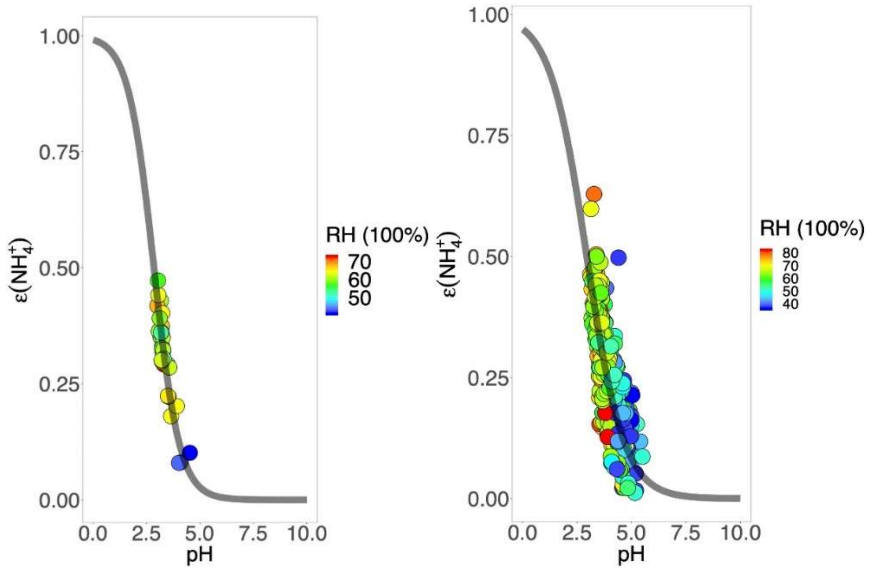

(a) (b)

Figure S10. $\varepsilon(NH_4^+)$ as a function of pH, with color scales corresponding to RH (%) and Boltzmann fitting line of (a) summer sample $\varepsilon(NO_3^-)^*$ constrained from 0.7 to 0.8, (b) all three season (spring, summer, winter) samples within a certain range of $\varepsilon(NO_3^-)^*$ (0.8-0.95) and RH (>36%). Most of the points with high RH are close to the curve.

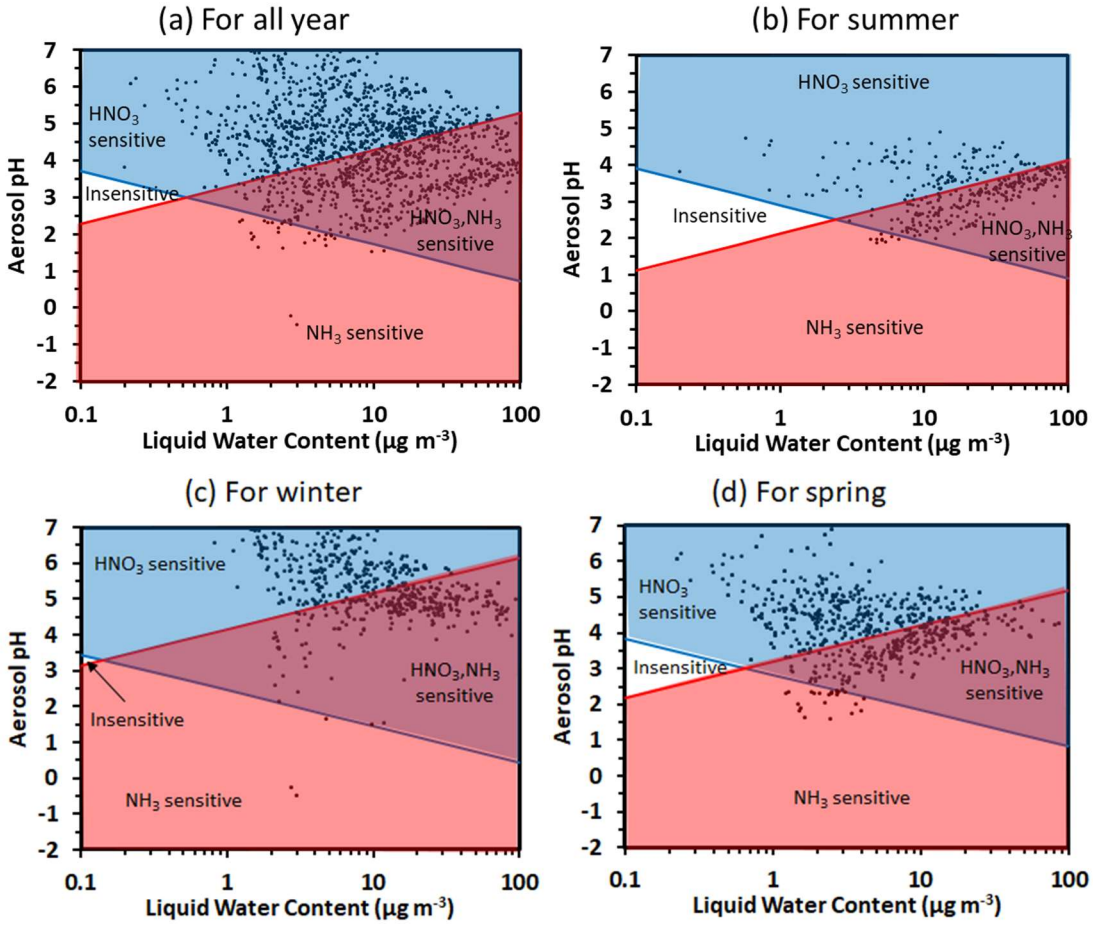

Figure S11. Sensitivity regime map for pH, HNO_3 and NH_3: (a) all year (summer, winter, spring), (b) summer, (c) winter, (d) spring. (The region lines (red and blue lines) for all samples and three seasons are calculated individually.)

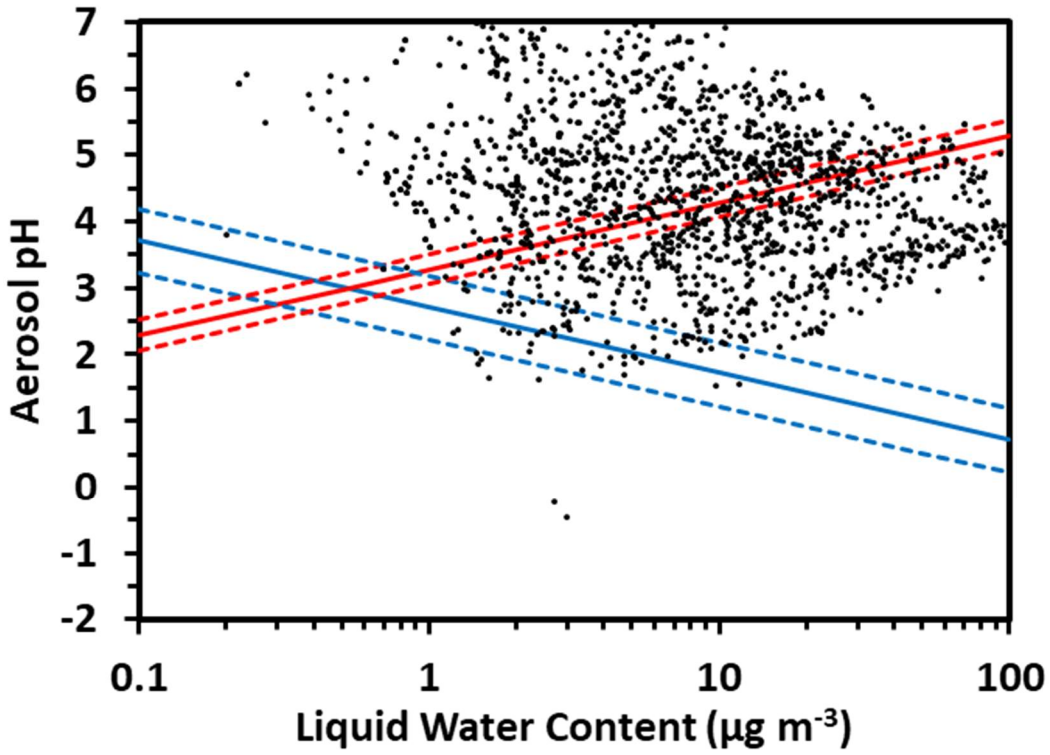

Figure S12. Sensitivity regime map of aerosol pH to NH_3 and HNO_3 for samples from the entire sampling period. The dotted lines show the sensitivity of temperature on the sensitivity regime map. The solid lines are calculated by average temperature of all samples, while the dotted lines are calculated by average temperature minus or plus the standard deviation of temperature of all samples.

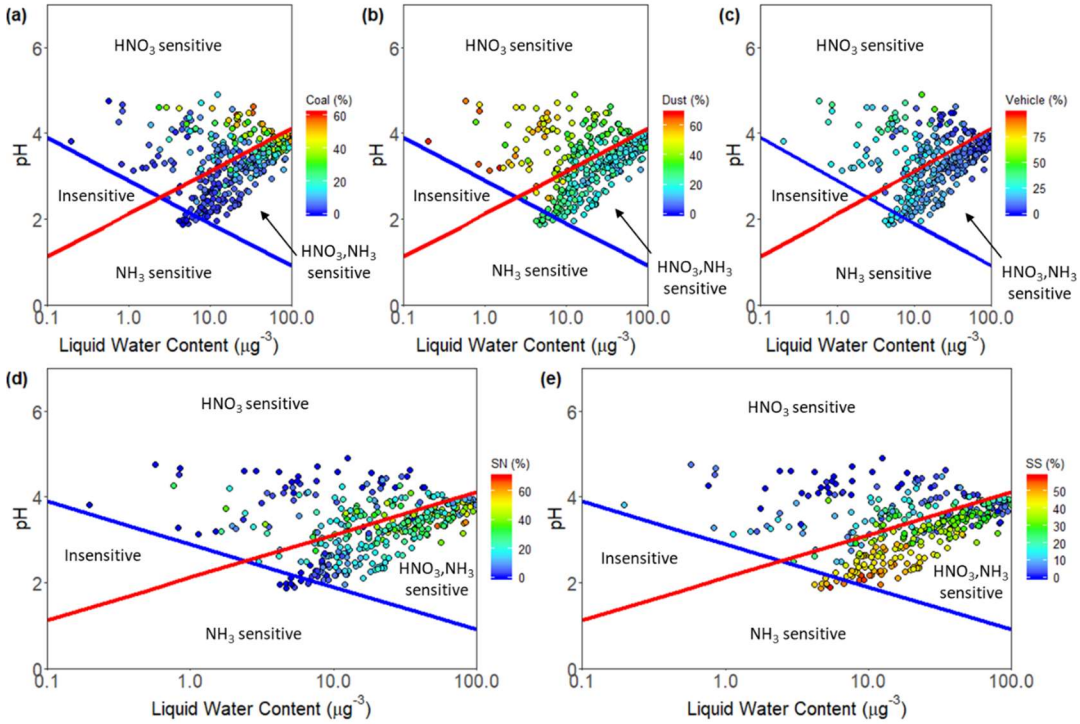

Figure S13. Joint source-NH_3/HNO_3 sensitivity of aerosol pH to NH_3 and HNO_3 for samples from summer. **(a)** Coal, **(b)** Dust, **(c)** Vehicle, **(d)** SN **(e)** SS.

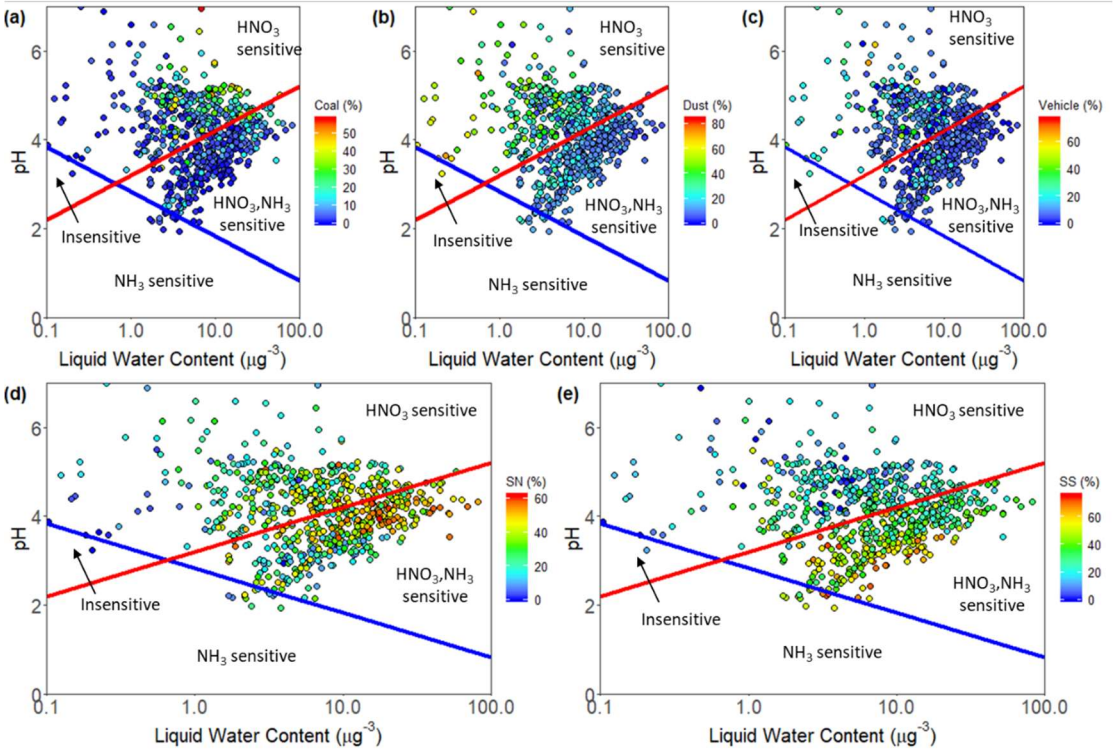

Figure S14. Joint source-NH_3/HNO_3 sensitivity of aerosol pH to NH_3 and HNO_3 for samples from spring. **(a)** Coal, **(b)** Dust, **(c)** Vehicle, **(d)** SN **(e)** SS.

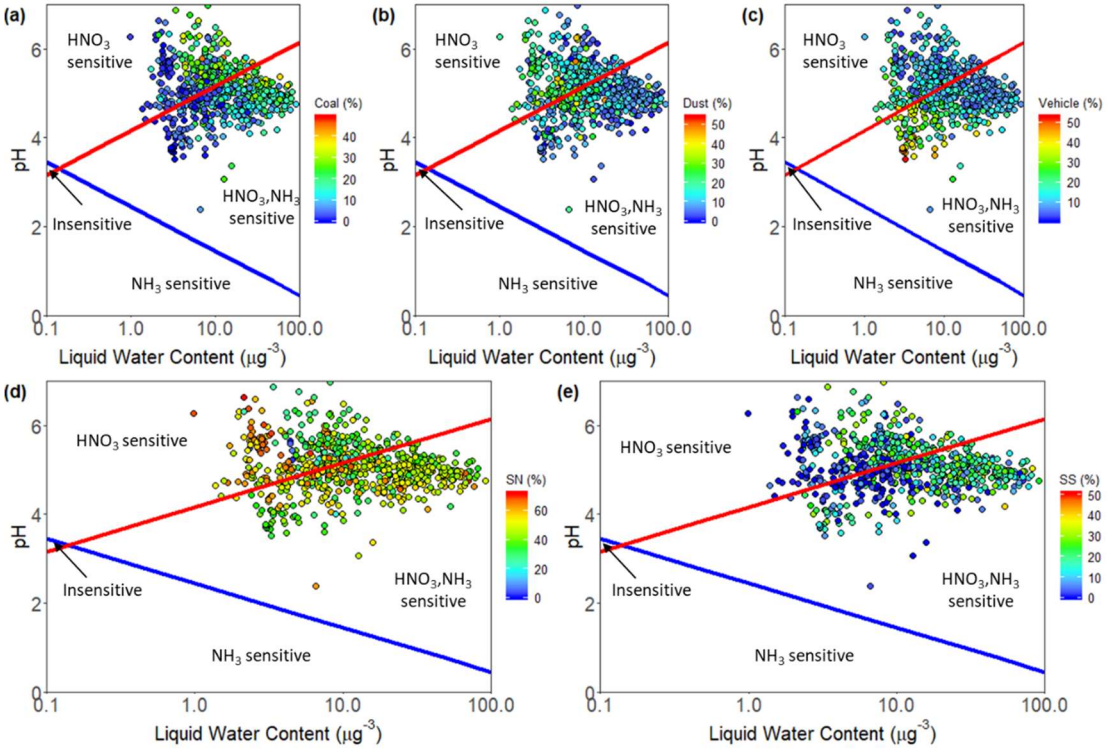

Figure S15. Joint source-NH_3/HNO_3 sensitivity of aerosol pH to NH_3 and HNO_3 for samples from winter. **(a)** Coal, **(b)** Dust, **(c)** Vehicle, **(d)** SN **(e)** SS.

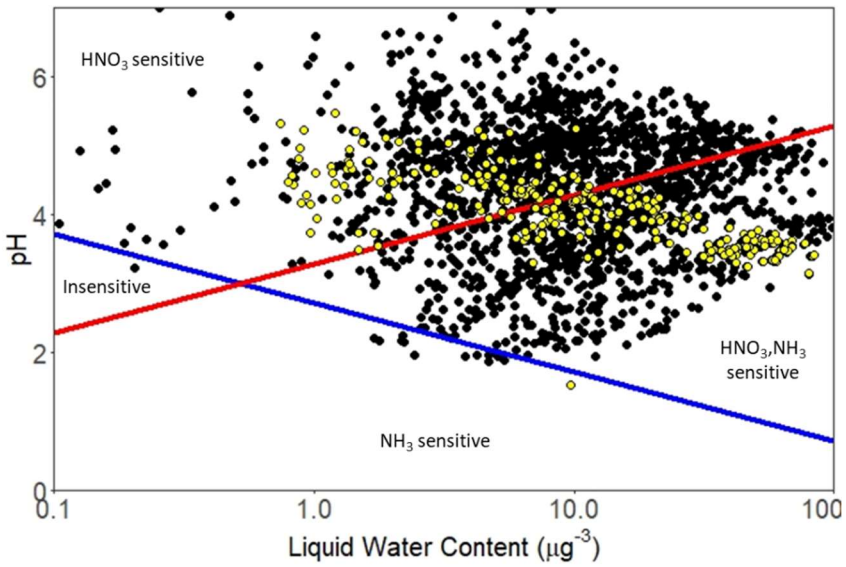

Figure S16. Sensitivity regime map of aerosol pH to NH_3 and HNO_3 for samples from the entire sampling period. The black points are the data collected from all year. The yellow points represent the data applied in Boltzmann fitting ($\varepsilon(NO_3^-)$* (0.8-0.95) and RH (>36%))

■REFERENCES

(66) Amato, F.; Pandolfi, M.; Escrig, A.; Querol, X.; Alastuey, A.; Pey, J.; Perez, N.; Hopke, P. K. Quantifying road dust resuspension in urban environment by Multilinear Engine: A comparison with PMF2. *Atmos. Environ.* **2009**, *43*, 2770-278.

(67) Amato, F.; Hopke, P. K. Source apportionment of the ambient PM2.5 across St. Louis using constrained positive matrix factorization. *Atmos. Environ.* **2012**, *46*, 329-337.